NASA Technical Paper 1834

Some Effects of Thermal-Cycle-Induced Deformation in Rocket Thrust Chambers

Ned P. Hannum and Harold G. Price, Jr.

APRIL 1981

NASA

NASA Technical Paper 1834

Some Effects of Thermal-Cycle-Induced Deformation in Rocket Thrust Chambers

Ned P. Hannum and Harold G. Price, Jr.
Lewis Research Center
Cleveland, Ohio

NASA
National Aeronautics
and Space Administration

**Scientific and Technical
Information Branch**

1981

A

Summary

A test program to investigate the deformation process observed in the hot-gas-side wall of rocket combustion chambers was conducted for three different liner materials. Five thrust chambers were cycled to failure by using hydrogen and oxygen as propellants at a chamber pressure of 4.14 MN/m^2 (600 psia). The deformation was observed nondestructively at midlife points and destructively after failure occurred. The cyclic life results are presented with an accompanying discussion about the problems of life prediction associated with the types of failures encountered in the present work. Data indicating the deformation of the thrust chamber liner as cycles are accumulated are presented for each of the test thrust chambers. From these deformation data and observation of the failure sites, it is evident that modeling the failure process as classic low-cycle thermal fatigue is inadequate as a life prediction method. The stress rupture model that has been proposed may apply to oxygen-free, high-conductivity (OFHC) copper but not to the other materials that were tested. Also, the effects of deformation and surface roughening on rocket thrust chamber wall temperatures were studied by using a thermal analysis computer program.

Introduction

The requirement for reusability of high-chamber-pressure, regeneratively cooled, rocket thrust chambers in the near future has precipitated experimental and analytical thermal fatigue studies related to thrust chamber life. The heat flux associated with the high-chamber-pressure (13.8 to 20.7 MN/m^2; 2000 to 3000 psia) engines cannot be accommodated by low-thermal-conductivity materials with the wall thicknesses necessary for the pressure loads. Therefore high-thermal-conductivity materials, such as copper or copper alloys, must be used for the thrust chamber walls. The expected design life for these thrust chambers is from 100 to 300 cycles. The work reported herein was an experimental investigation to study some of the effects of the wall deformation that occurs during cyclic testing of high-conductivity thrust chambers.

In 1972, low-cycle thermal fatigue tests were conducted by the U.S. Air Force with rocket combustion chambers that had been designed and fabricated by Rocketdyne (refs. 1 and 2). These tests were conducted at a chamber pressure of 5.2 MN/m^2 (750 psia). Experimental fatigue life was compared without success with the analytical predictions of life for two zirconium-copper alloy thrust chambers. The NASA Marshall Space Flight Center later acquired more of these chambers and continued the work. The life analysis for these tests is reported in reference 3.

In the previous work the life-limiting failure mechanism was thought to be low-cycle thermal fatigue. The controlling parameters were therefore the temperature difference between the hot-gas-side wall surface and the outside wall surface, the coefficient of thermal expansion for the liner materials, and the geometry of the thrust chamber liner. The fatigue life was then related to the strain range that occurs in the liner during a thermal cycle. The finite element models used to compute strain range assumed that the geometry remained fixed throughout the life of the thrust chamber.

In 1973 work began at the Lewis Research Center to systematically investigate the problem of thrust chamber life. The approach was to use cyclic testing under controlled conditions and with a test procedure designed specifically to study thrust chamber life. Inexpensive cylinders with plug nozzles were used to evaluate various thrust chamber liner materials over a range of hot-gas-side wall temperatures. These experimental life data were correlated both with the hot-gas-side wall temperature and the temperature difference between the hot-gas-side surface and the outside surface of the liner wall for each material tested (ref. 4). Finite element analyses were conducted to compute strain range. Attempts were made to predict life by assuming a low-cycle-thermal-fatigue failure mechanism and using life data from uniaxial isothermal fatigue tests as a reference. This life prediction procedure was generally not successful for either the cylindrical thrust chambers of reference 4 or the contoured thrust chambers of reference 5. The analysis did indicate, however, that reducing the stiffness of the outer wall structure (closeout) of the thrust chamber could reduce the strain range. Contoured thrust chambers were then fabricated and tested to experimentally investigate this predicted trend. The closeout stiffness was reduced by replacing most of the thick, electroformed closeout with a fiberglass wrap, and an increase in life was observed (ref. 6).

Life can also be increased by decreasing the hot-gas-side wall temperature, as reported in reference 4 and as shown by various analytical studies. Life was also improved experimentally by applying a coating

to the hot-gas-side surface of cylindrical thrust chambers to reduce the temperature of the metal thrust chamber liner (ref. 7).

Although some success has been achieved in predicting trends, an *a priori* life prediction was still not possible, apparently because the failure mechanism was not properly described by the low-cycle thermal fatigue model assumed in the analysis. A more detailed description of the behavior of the thrust chamber hot-gas-side wall near the failure site is needed to contribute to understanding of the failure mechanism.

In response to this need five thrust chambers were fabricated from three different liner materials and tested. The objectives of the experimental investigation were (1) to obtain hot-gas-side wall deformation data throughout the life span of rocket thrust chambers, (2) to obtain cyclic life and hot-gas-side wall deformation data for different liner materials, and (3) to evaluate the effects that accumulated deformation has on the temperature distribution within the structure. In the course of this investigation nondestructive methods were used for locating potential failure sites early in the life of a thrust chamber and for making periodic measurements of the deformation.

The thrust chambers used in this investigation had a throat diameter of 6.60 centimeters (2.60 in.) and were operated at a chamber pressure of 4.14 MN/m^2 (600 psia). The propellants were liquid oxygen and gaseous hydrogen. The chambers were cooled with a separate flow of liquid hydrogen. The thrust chambers were made with fabrication methods that are typical for high-pressure, high-performance rocket engines such as the Space Shuttle Main Engine. Coolant passages were milled into a high-thermal-conductivity liner. Nickel was then electrodeposited onto the liner to close out the coolant channel and form the outer structural jacket.

Apparatus

Test Facility

The investigation was conducted at the Lewis Research Center rocket engine test facility. This is a 222 410-newton (50 000-lbf), sea-level rocket test stand equipped with an exhaust-gas muffler and scrubber. The facility used pressurized propellant-storage tanks to supply the propellants to the combustor. Propellants for combustion were liquid oxygen and ambient-temperature gaseous hydrogen. Liquid hydrogen was used as the thrust chamber coolant. Details of the installation are shown in figure 1. Figure 1(a) shows the thrust stand and exhaust-gas scrubber with a typical combustion chamber mounted in place. Figure 1(b) is a schematic of the test facility that shows the propellant supply and the instrumentation locations.

A separate coolant flow circuit was used to allow coolant flow to be independent of engine propellant flow. The spent hydrogen coolant was disposed of through a burn stack. For test convenience, an external ignitor torch was used to ignite the propellants. At ignition the flame front would pass upward through the throat and ignite the propellants in the combustion chamber.

Injectors

With the all-flow-through injector design used in this investigation all of the fuel (gaseous hydrogen) was injected through a porous Rigimesh face plate. The oxidant was injected through 85 showerhead tubes distributed evenly over the injector face. Figure 2(a) shows the face side of an injector; figure 2(b) is a cross-sectional sketch of one element, showing the liquid-oxygen tube and the porous face through which the fuel was injected.

Fatigue Combustion Chambers

The details of the thrust chambers used in the low-cycle fatigue life investigation are shown in figure 3. The chamber contour is shown in figure 3(a). The chambers, which had a contraction ratio of 3.70, were 38.1 centimeters (15 in.) long overall, with the throat located 25.4 centimeters (10 in.) from the injector face. The throat was 6.60 centimeters (2.6 in.) in diameter, and the nozzle exit was 13.2 centimeters (5.2 in.) in diameter. The chamber liners were made of copper or copper alloys and had coolant passages machined into the outer surface (fig. 3(b)). After machining, the coolant passages were temporarily filled with a wax, and a layer of nickel was electrodeposited onto the outer surface to close out the coolant channels and form the outer structural jacket. The coolant passage cross section thus formed is shown in figure 3(c), which is a section through the throat plane of the chamber. The coolant passage dimensions were selected to provide a hot-gas-side wall temperature of 811 K (1460° R) in the throat for the operating conditions of 4.14-MN/m^2 (600-psia) chamber pressure and 0.91-kg/sec (2.0-lb/sec) coolant flow rate. Much lower temperatures were selected for other areas of the chamber to ensure that the throat would be the region of highest strain. All chambers used in the testing were designed with the same coolant passage height at the throat section. After electroforming of the closeout the wax was melted out of the coolant

(a) Test combustion chamber and thrust stand.

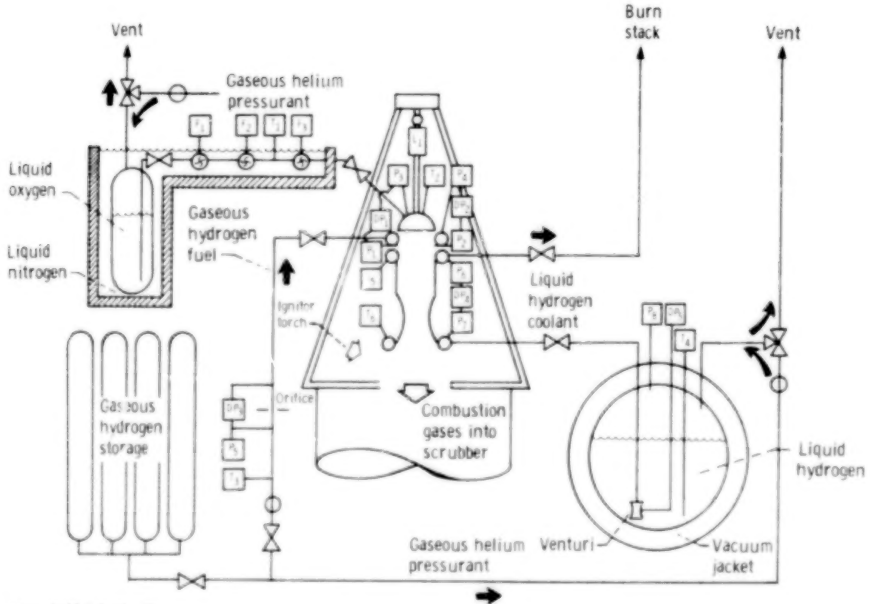

L_1 Thrust; strain-gage, bridge load cell

F_1, F_2, F_3 Oxidizer flow; turbine flowmeter

P_1, P_2 Combustion chamber pressure; strain-gage, bridge pressure transducer

P_3 Oxidizer injection pressure; strain-gage, bridge pressure transducer

P_4 Fuel injection pressure; strain-gage, bridge pressure transducer

P_5 Fuel orifice pressure; strain-gage, bridge pressure transducer

P_6 Coolant outlet pressure; strain-gage, bridge pressure transducer

P_7 Coolant inlet pressure; strain-gage, bridge pressure transducer

P_8 Coolant tank pressure; strain-gage, bridge pressure transducer

T_1 Oxidizer temperature at flowmeters; platinum resistance bridge transducer

T_2 Oxidizer injection temperature; platinum resistance bridge transducer

T_3 Fuel temperature at orifice; copper-constantan thermocouple

T_4 Coolant temperature at venturi; platinum resistance bridge transducer

T_5 Coolant outlet temperature; Chromel-constantan thermocouple

T_6 Coolant inlet temperature; platinum resistance bridge transducer

DP_1 Oxidizer injector pressure drop; strain-gage, bridge pressure transducer

DP_2 Fuel injector pressure drop; strain-gage, bridge pressure transducer

DP_3 Fuel orifice pressure drop; strain-gage, bridge pressure transducer

DP_4 Coolant jacket pressure drop; strain-gage, bridge pressure transducer

DP_5 Coolant venturi pressure drop; strain-gage, bridge pressure transducer

(b) Schematic of test facility.

Figure 1. - Test facility.

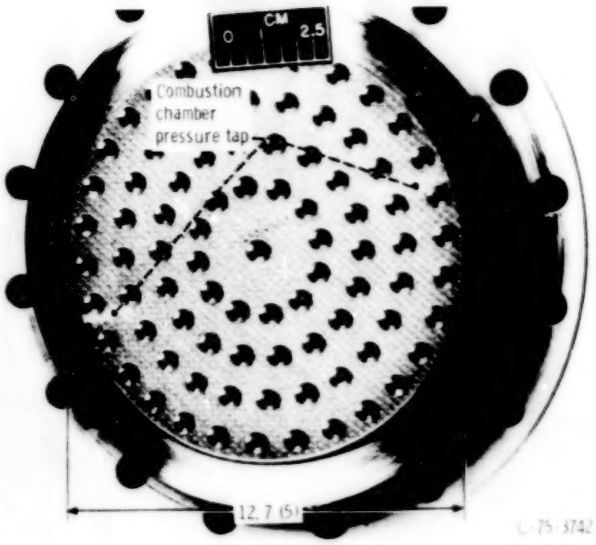

(a) Injector face.

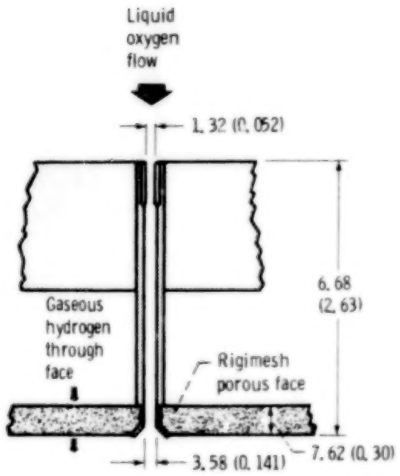

(b) Sketch of injector element.

Figure 2. - Injector. (Dimensions are in centimeters (in.).)

passages, the manifolds were welded on, and the instrumentation was attached. Figure 3(d) shows a completed chamber.

A different closeout procedure was used for the two oxygen-free, high-conductivity (OFHC) liners reported in the present work than that described above. Instead of the relatively thick (0.485 cm, 0.191 in.) nickel closeout the OFHC liners were closed out with a two-part, low-stiffness structure composed of a thin, electroformed copper closeout and a fiberglass overwrap for hoop strength. All other dimensions and details were the same as those described above. The specific details of these low-stiffness OFHC copper chambers are further described in reference 6.

Combustion Chamber Liner Materials

The liner materials were OFHC copper or copper alloys. One alloy was copper with 0.15 percent zirconium, available from AMAX Corporation as Amzirc. The other alloy was copper with 0.45 percent zirconium and 3 percent silver, available from Rocketdyne as Narloy-Z. The OFHC copper liner material was in the as-forged condition. The Narloy-Z liners were solution annealed and aged after machining. The Amzirc liner was fabricated with the material in the heat-treated condition. The serial number, liner material, and material condition of the chambers used in this investigation are listed in table I. Two OFHC copper, two Narloy-Z, and one heat-treated Amzirc liner were tested.

Thrust Chamber Wall Instrumentation

The thrust chambers were instrumented with two types of thermocouples. Copper-constantan alloy thermocouples were spot welded onto the outside surface of the combustion chamber. And high-response Chromel-constantan thermocouples were inserted into small holes in the cooling passage ribs to measure wall temperature. The thermocouple tip was located within 1.27 millimeters (0.050 in.) of the hot-gas-side wall surface (chamber inside surface).

A sectional view showing a typical rib thermocouple hole is presented in figure 3(c). Inspection of the precision-machined holes indicated that the distance from the bottom of the hole to the hot-gas-side surface was 1.27 ± 0.05 millimeters (0.05 ± 0.002 in.). Analysis has shown that the temperature profile across the rib at this radial station is essentially flat, and precision in circumferential location of the thermocouple hole is necessary only to keep from breaking into a coolant passage. To make sure that the thermocouple holes did not break into the coolant passages, each was leak tested with helium.

The rib thermocouple was fabricated by inserting 0.025-millimeter (0.001-in.) diameter Chromel and constantan wires into 0.35-millimeter (0.014-in.) diameter stainless-steel tubing. A junction was formed at the end of the tube in a small "bullet"-shaped tip of silver solder. The probe tip was then gold plated with a thickness of approximately 0.005 millimeter (0.0002 in.) in order to provide a malleable contact surface to press against the copper at the bottom of the hole in the rib. The probe was then spring loaded against the hole bottom with a force of approximately 120 grams (0.26 lb). When the rib temperature probes were initially used in the test program, the useful life was limited by a thin corrosion film that formed in the

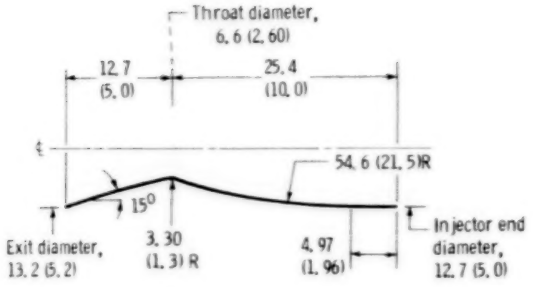

(a) Chamber contour.

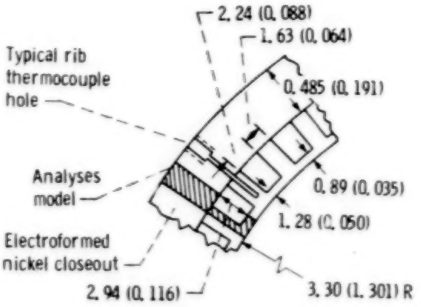

(c) Throat cross section.

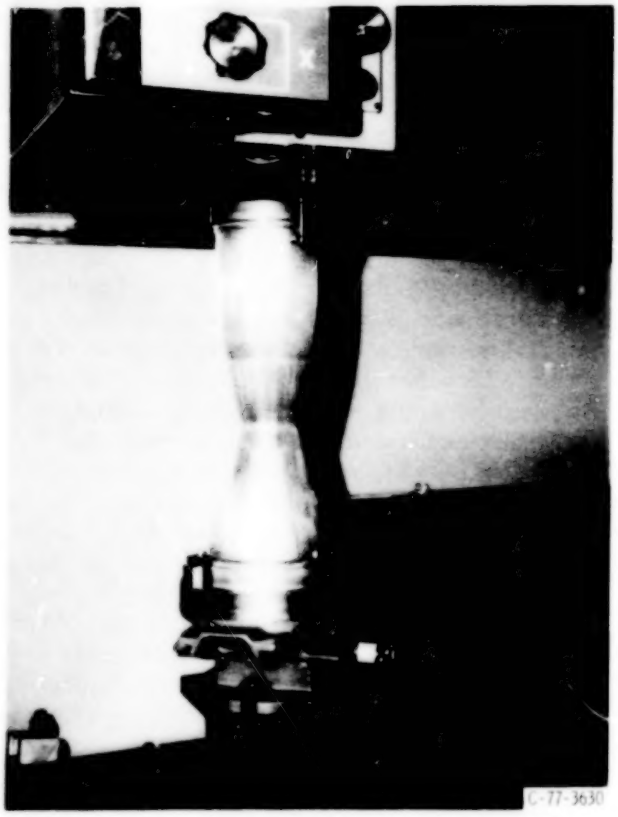

(b) Thrust chamber liner showing milled coolant channels before addition of electroformed closeout.

(d) Completed fatigue chamber.

Figure 3. - Fatigue chambers.

thermocouple hole and caused a change in both the response rate and the accuracy.

A model for this corrosion process is offered as follows: The outside surface of the chamber would cycle from below 55 K (100° R) between firings to above 222 K (400° R) while firing. The thermocouple holes would cryopump condensable gases, which would then evaporate from the holes during each cycle. The temperature reading was thus being affected by both the heat of condensation (and evaporation) of these condensable gases and by the presence of surface corrosion that formed as a result of the environment. To avoid this problem, a flow of low-pressure (17.2 kN/m^2; 2.5 psig) gaseous helium was used to effectively displace any condensable gases from the entrance to the thermocouple holes. This method proved to be effective, as indicated by the continued fast-response characteristics of the temperature probe. Rib temperature probes were installed on new thrust chambers and provided useful data throughout the life of the chamber.

Procedure

The test cycle selected for this program is shown in figures 4 and 5. In this cycle the maximum temperature difference between the hot-gas-side wall

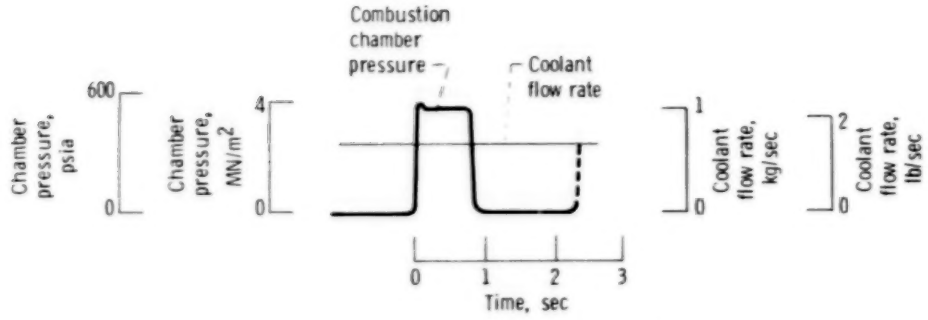

Figure 4. - Schematic of duty cycle used in testing of rocket chambers.

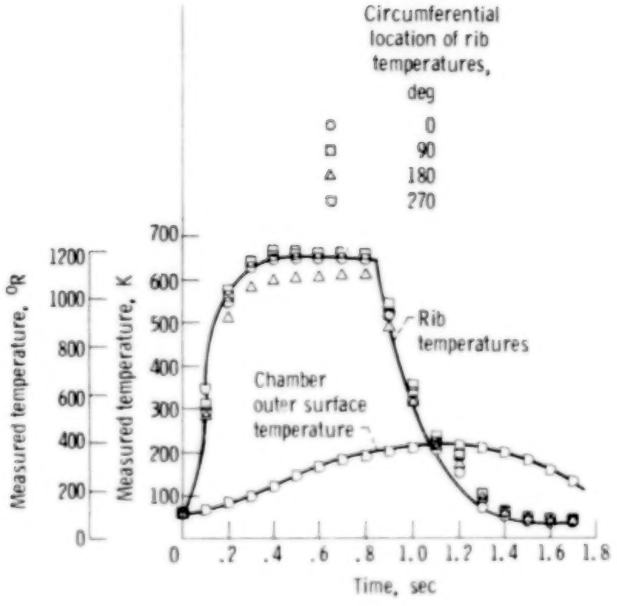

Figure 5. - Measured throat-plane rib temperature and chamber outer surface temperature as a function of time for one firing cycle.

and the chamber outside surface occurred during the fast start transient. The combustion chamber reached full chamber pressure in 0.05 to 0.06 second. The maximum temperature difference across the wall was achieved 0.3 second after start and was equal to approximately 130 percent of the steady-state value. Once the test firing was well beyond the time when the maximum temperature difference had occurred, the chamber was shut down. This gave a rated thrust duration of about 0.85 second. The liquid-hydrogen coolant flow was continued during a 1.4 second shutdown period, which was enough time to cool all parts of the chamber to original temperature conditions. Then the chamber was recycled. This gave a total cycle duration of 2.3 seconds. The propellant storage capability of the facility permitted as many as 125 cycles in a single firing series.

The test cycle was programmed into a solid-state timer that was accurate and repeatable to within ±0.001 second. Fuel and oxidizer flows were controlled by fixed-position valves and propellant tank pressures. Coolant flow was controlled by a cavitating venturi. Coolant inlet pressure was controlled by coolant tank pressure, and coolant exit pressure was kept constant by a closed-loop controller modulating a backpressure valve. Control room operation of the test included monitoring of the test hardware by means of three closed-circuit television cameras and one cell microphone.

The outputs of the microphone and one television camera were recorded on magnetic tape for later playback. The cell microphone was the primary data sensor for determining the time of the fatigue failure. During the cooldown phase of the cycle any coolant leak through the wall into the combustion chamber could be heard very clearly. In most cases it was possible to recognize that the thrust chamber wall had cracked and to stop the cyclic testing within two cycles after the crack occurred. During playback of the audio tape the exact cycle when the crack occurred could be precisely determined.

After every series of test cycles gaseous helium was introduced into the coolant channels remotely and was trapped there under pressure. The presence of a pressure decay would indicate the presence of a crack. If a crack was indicated, the facility was shut down and the crack was located by direct observation. Methods for measuring the deformation of the thrust chamber liner both on the test stand and in an inspection facility were developed and are described in the Results and Discussion section. These methods were used both at intermediate-life points and for postfailure data.

Results and Discussion

Experimental results are presented from the testing of five rocket thrust chambers. Tests consisted of

repeated firings of each rocket thrust chamber until a crack occurred in the liner wall and allowed coolant to leak into the combustion chamber. After the combustion performance and stability characteristics are discussed, typical test conditions are presented. The cyclic life results are presented with an accompanying discussion about the problems of life prediction associated with the types of cracks encountered in the present work. Data indicating the deformation of the thrust chamber liner as cycles are accumulated are presented for each test thrust chamber. Also a description of the computer program used in the thermal design of the thrust chambers and in the analysis of the data is included. This thermal design computer program is also used to study the effects of deformation and surface roughening on the temperature of the rocket thrust chamber wall.

Combustion Performance and Stability

The all-flow-through injector design described in the Apparatus section had excellent performance, heat flux uniformity, stability, and durability characteristics. The heat flux uniformity of the injector was determined by conducting firing tests with ablative chambers and examining the erosion patterns. Comparative tests were made with both concentric-tube and all-flow-through injectors, each with the same number and location of elements. The erosion rate was significantly more uniform, both near the injector and in the throat region, with the all-flow-through design indicating a more uniform heat flux. The energy release efficiency, which was determined from short-duration tests with heat-sink thrust chambers, was 97.5 percent with all data within a scatter band of ± 0.5 percent. The performance procedure used to compute injector efficiency is outlined in reference 8.

During the performance testing with the heat-sink thrust chambers tests were made with high-response piezoelectric pressure transducers installed on the thrust chamber in order to measure combustion chamber pressure oscillations and thereby to ascertain whether combustion instability was present. No instability was found.

Test Conditions

The chamber pressure test cycle used for the life evaluation of the various chambers is described in the Procedure section and shown in figure 4. The nominal steady-state combustion chamber pressure was 4.14 MN/m^2 (600 psia), and the nominal coolant flow rate was 0.91 kg/sec (2.0 lb/sec). Care was taken to ensure that the combustion propellent and coolant flow rates and pressures were nearly the same for each cycle of a test series. The steady-state oxidant-fuel ratio was nominally 6.0 and was held within a range of approximately ± 0.15 for all tests. Combustion chamber pressure did not vary more than ± 3 percent from the nominal value. Coolant flow rate did not vary more than ± 2 percent from the nominal value. Experimental data reported in reference 9 have shown that a ± 2 percent variation in coolant flow rate is equivalent to a ± 11 kelvin (± 20 deg R) variation in rib temperature measured 1.27 millimeters (0.050 in.) back from the hot-gas-side wall.

Typical rib temperature data for a single cycle are presented in figure 5. The data presented are typical of all chambers tested in terms of transient response and the range of data between the four thermocouples. The difference in temperature between the hottest and the coldest circumferential locations was approximately 69 K (125 deg F) at the end of the transient and less than that toward the end of the firing. The rise time for the chamber pressure transient was approximately 0.4 second. Also shown in figure 5 is a typical chamber outer surface temperature as a function of time for one firing cycle. It can be seen that this parameter does not come to steady state during the short-duration cycle.

Comparison of Failure Sites with Analytical Model

In studies reported in references 3 to 5 thrust chamber cyclic life has been approached analytically as a low-cycle thermal fatigue problem. For the low-cycle thermal fatigue model the temperature difference across the liner wall and the coefficient of thermal expansion were used in a finite-element computer program to compute strain range.

The strain range was computed in reference 5 with this method for a thrust chamber configuration and duty cycle identical to those for the heat-treated Amzirc and Narloy-Z thrust chambers tested in the present work. It was shown in reference 5 that the effect of liner material on computed strain range was small for the copper and copper alloy materials analyzed. This is because most of the strain is produced by the thermal forces and is therefore only a function of the coefficient of thermal expansion and the temperature distribution across the hot-gas-side wall, both of which are virtually the same in all the copper and copper-based alloy materials tested. The average computed strain range in the thin hot-gas-side wall over the coolant channels was 2.5 percent for the heat-treated Amzirc chamber (serial number 82) and also for the Narloy-Z chambers (serial numbers 140 and 150). It was noted in the Fatigue Combustion Chambers section that the

OFHC copper chambers (serial numbers 74 and 75) were fabricated by using a different closeout technique. It was reported in reference 6 that the reduced stiffness of the OFHC chamber closeout reduced the computed strain range in the throat region to 2.3 percent.

From the uniaxial isothermal fatigue results in reference 9 and the computed strain range, the predicted life of the heat-treated Amzirc chamber is 500 cycles, and the prediced life of the OFHC copper chambers is 200 cycles. From similar life data (ref. 10) the predicted life of the Narloy-Z chambers is 200 cycles.

The assumptions that were made in arriving at these life predictions were (1) that the geometry and consequently the temperature distribution remained fixed over the entire life of the chamber and (2) that the failure mechanism is low-cycle fatigue. As the data base increases for rocket thrust chambers that have been cycled to failure (refs. 1, 2, and 4 to 7) it is clear from the postfailure inspections that the assumption of fixed geometry is not realistic and further that the failure mechanism is most likely not classic low-cycle fatigue.

Description of Failure Sites

The crack sites were generally characterized by a thinning and bulging of the hot-gas-side wall. Also, there was a roughening of the hot-gas-side wall, especially in the throat region of the thrust chamber. Figure 6(a) is a view of the hot-gas-side wall showing the general surface roughening of OFHC copper chamber 74. A 3.5-centimeter (1.4-in.) long crack at the centerline of a coolant channel can also be seen. A post-test inspection of all the chambers tested revealed that the roughening was more severe with the OFHC copper than with the Narloy-Z and the heat-treated Amzirc. Also, the roughening was more severe in the throat region, where the temperature was higher than at other locations in the combustion chamber.

A cross section, at the throat, of an entire thrust chamber is shown in figure 6(b). This is OFHC copper chamber 74, which had the low-stiffness closeout described in the Apparatus section. The fiberglass portion of the closeout has been removed. It can be seen in figure 6(b) that the deformation is not the same in each of the 60 coolant channels. The circumferential location of the most severe deformation seems to be random, that is, not related to injector patterns, cooling manifolds, or fabrication anomalies that are within the drawing specifications.

Cross-sectional views of the failure sites for two different materials are shown in figure 7. The failed

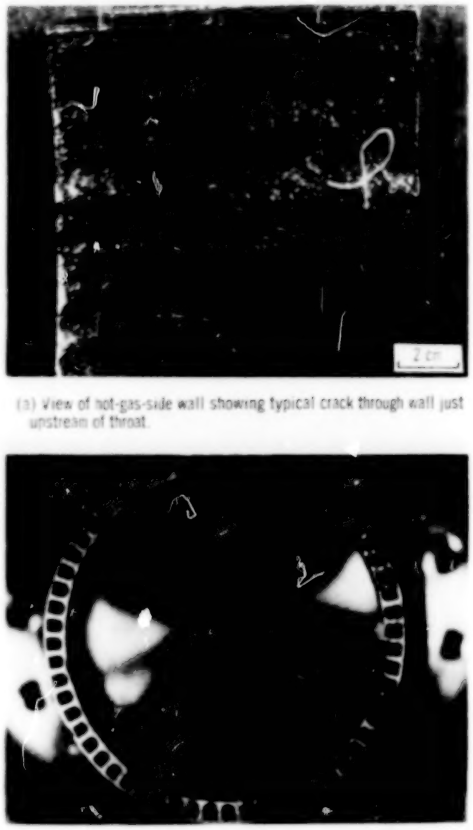

(a) View of hot-gas-side wall showing typical crack through wall just upstream of throat.

(b) Cross section of throat plane showing 60 cooling channels and electroformed closeout.

Figure 6. - OFHC copper thrust chamber 74, typical failure site and deformation of hot-gas-side wall.

coolant channel is characterized by a "doghouse" shape and a bulge of the hot-gas-side wall toward the centerline of the thrust chamber. Conservation of the wall material was assumed since no hot-gas-side surface melt or erosion was observed. The hot-gas-side wall must thin therefore to accommodate the bulge. Because of the progressive thinning a valley tends to form at the center of each bulge to form two bumps per cooling channel. It can be seen in figure 7(a) that much greater bulging and thinning occurred with the OFHC copper material than with Narloy-Z (fig. 7(b)). The failure sites for the other thrust chambers (not shown) also had the doghouse shape. Although all materials deformed similarly, an important difference is evident between the two failure sites shown in figure 7. In addition to the thinning of the hot-gas-side wall, a necking of the material in a small region on each side of the failure site occurred with the OFHC copper. This is the typical appearance of a tensile failure with a ductile material. Tensile failures were observed in reference 4 for OFHC copper, heat-treated Amzirc, and Narloy-Z. The failure mechanism was described as stress rupture. In the present work the failure site

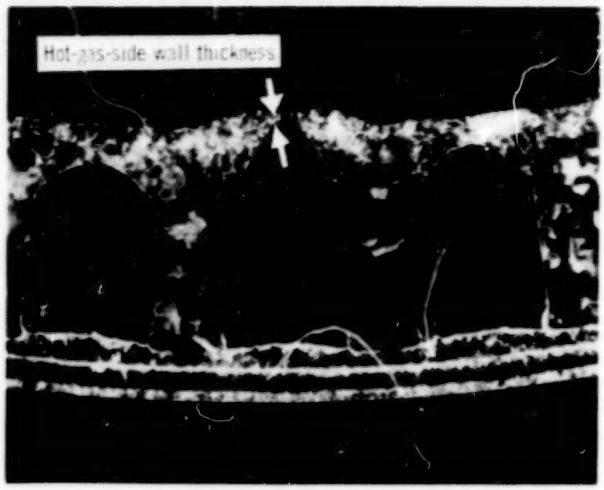

(a) OFHC copper thrust chamber 75.

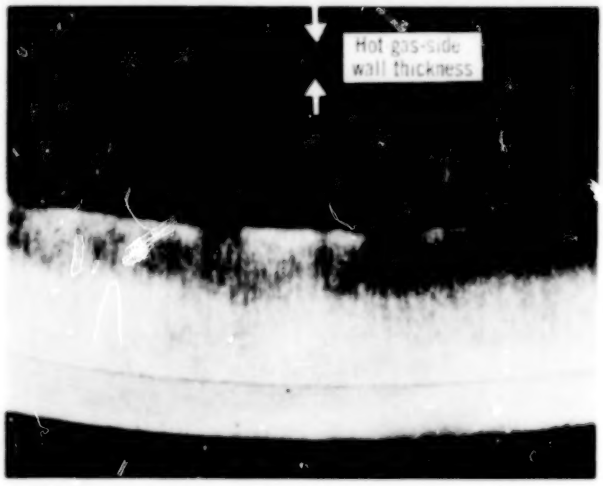

(b) Narloy-Z thrust chamber 150.

Figure 7. - Cross-sectional view of failure sites.

shown for Narloy-Z in figure 7(b) does not show necking of the material adjacent to the crack. Therefore the visual evidence in the present work supports the reference 4 contention of a tensile stress failure mechanism only with OFHC copper. The failure sites of the Narloy-Z and heat-treated Amzirc in the present work are different than those observed in reference 4 because there is no evidence of necking adjacent to the crack with these materials. The failure mechanism for Narloy-Z and heat-treated Amzirc appears therefore to be more fatigue related.

Cycles to Failure

For this investigation a fatigue failure was defined as a crack through the hot-gas-side wall that permitted audible detection of a coolant leak into the combustion chamber during the nonfiring portion of the cycle. Cracks of approximately 1000 micrometers (0.039 in.) in length were the minimum size detected by this method. Most tests were manually aborted within one or two cycles after it was suspected that a failure had occurred. The coolant passages were then inspected to determine the number and location (or locations) of the failures.

The experimentally determined cyclic life for each of the five chambers tested in this program is given in table I. One of the two Narloy-Z chambers (serial number 140) failed after 301 cycles. The second Narloy-Z chamber (serial number 150) failed after 154 cycles. After 250 cycles inspection of the heat-treated Amzirc chamber (serial number 82) revealed three very small pin holes and one small crack. Therefore there is some uncertainty about the exact cycle in which failure occurred. The two OFHC copper chambers (serial numbers 74 and 75) failed at 193 and 202 cycles, respectively.

Comparison of the experimentally determined life with the predicted values presented earlier gave rather typical results. The experimentally determined life with the two OFHC copper chambers was twice the predicted life; the Amzirc chamber life was one-half of predicted. The predicted life for the Narloy-Z chamber was between the two experimental values. As stated earlier a life prediction model that ignores the progressive deformation that occurs in milled-channel thrust chambers with electroformed closeouts is of very limited value. Any attempt to upgrade the analytical life prediction methods was beyond the scope of the present work. However, attempts at modeling the deformation process and at correlating the predictions with experimental data have been reported in reference 11.

Effect of Cyclic Testing on Material Properties

Some metallographic observations were made of the material at the failure sites. It appears that some recrystallization has occurred in the hot-gas-side wall of OFHC copper chamber 75 (fig. 7(a)). No recrystallization was observed for the other materials. When hardness surveys were taken across sections similar to those shown in figure 7, it was found that the hardness adjacent to the failure site was different from the hardness away from the failure site (near the electroformed closeout). If it is assumed that the liner material away from the failure site remained in the pretest condition, then a change in hardness must have occurred at the failure site for all the liner materials during cyclic testing. Hardness measurements for each chamber are given in table I. The as-fabricated hardness with OFHC copper was R_B 12 to 15. At the failure sites there was softening

TABLE I. - DETAILS OF THRUST CHAMBER LINERS

Thrust chamber material	Serial number	Failure site deformation				Failure site wall thickness		Accumulated cycles	Material hardness, R_B	
		From polar plots		From photographs					As fabricated	Failure site
		mm	in.	mm	in.	mm	in.			
Narloy-Z	140	0.196	0.0077	0.196	0.0077	0.592	0.0233	[a]301	33	57
Narloy-Z	150	.135	.0053	.135	.0055	.650	.0256	[a]154	45	60
Heat-treated Amzirc	82	.030	.0012	-----	------	-----	------	99	--	--
		.135	.0053	.089	.0035	.711	.028	[a, b]250	10	15
OFHC copper	74	.160	.0063	-----	------	-----	------	114	--	--
		.173	.0068	-----	------	-----	------	124	--	--
		.155	.0061	-----	------	-----	------	[c]124	--	--
		.183	.0072	-----	------	-----	------	[c]154	--	--
		.216	.0085	-----	------	-----	------	[c]184	--	--
		.404	.0159	.399	.0157	.290	.0114	[a]193	15	9
OFHC copper	75	.091	.0036	-----	------	-----	------	94	--	--
		.361	.0142	.356	.0140	.277	.0109	[a]202	12	<0

[a]Postfailure data.

[b]Cycles to failure uncertain.

[c]Data from plaster cast.

to R_B 0 to 9. In contrast the heat-treated Amzirc and Narloy-Z hardened as cycles were accumulated. Heat-treated Amzirc hardened from R_B 10 to R_B 15; Narloy-Z chamber 140 hardened from R_B 33 to R_B 57. Narloy-Z chamber 150 hardened from R_B 45 to R_B 60. An observation can be made that both Narloy-Z chambers failed at about the same hardness, but the one that hardened more (R_B 33 to 57) had longer life (301 cycles as compared with 154 cycles). The reasons for these differences in material behavior are not understood. However, the isothermal fatigue data reported in references 9 and 10 also indicated similar changes in hardness as these materials were cycled.

Effect of Materials on Deformation Rate

Measurements of the deformation were made by nondestructive methods. After the thrust chamber was removed from the test stand, the chamber was centered on a turntable and a stylus was held against the inside surface at a known axial location. The stylus was connected to a piezoelectric type of micrometer that in turn displaced a marking stylus. Polar graph paper was rotated under the marking stylus by a linkage that connected the two turntables. The resulting plots of wall deformation are shown in figure 8. The calibration is approximately 20 times more sensitive in the radial direction than in the circumferential direction; consequently, the plots give a distorted view of the wall deformation. In most cases plots were made at several axial locations at or near the failure site. Reference plots were made for each chamber before hot testing, and no deformation was observed.

Polar plots were made for each of the thrust chambers to document the post-test hot-gas-side wall deformation. The hot-gas-side wall deformation for OFHC copper chamber 74 is presented in figure 8(a). The failure site and one or two other channels exhibit the double-bump characteristic. (Each cooling channel covers a 6° arc.) The deformation at the failure site is much greater than that at other locations in the thrust chamber. This was true for all materials, as shown in figure 8(c) for Narloy-Z chamber 140 and in figure 8(d) for heat-treated Amzirc chamber 82. The deformation data from these polar plots are tabulated in table I. Deformation at the failure site was defined as the distance from the valley (at approxiately the rib centerline) to the largest peak. The data tabulated were for the largest observed hot-gas-side wall deformation measured from plots such as figure 8(a).

Since the method for measuring deformation was

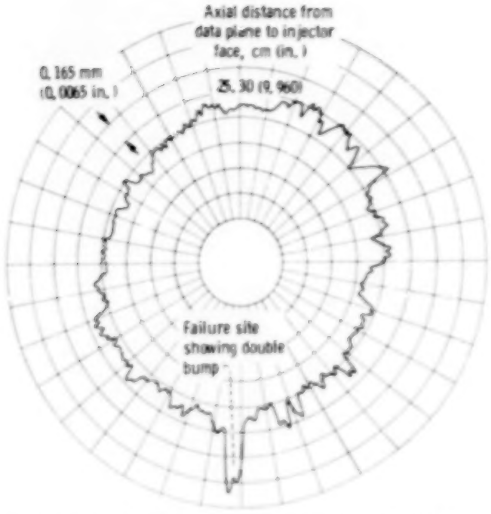

(a) Postfailure data for OFHC copper thrust chamber 74 after 193 cycles.

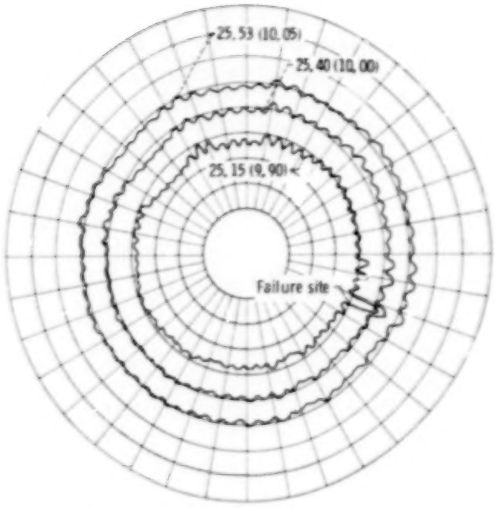

(c) Postfailure data for Narloy-Z thrust chamber 140 after 301 cycles.

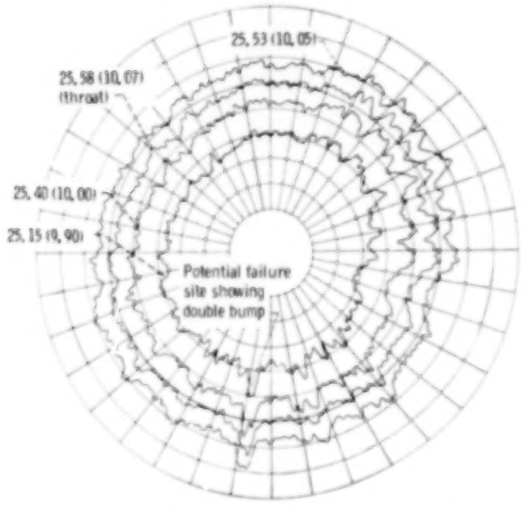

(b) Intermediate-life data for OFHC copper thrust chamber 74 after 124 cycles.

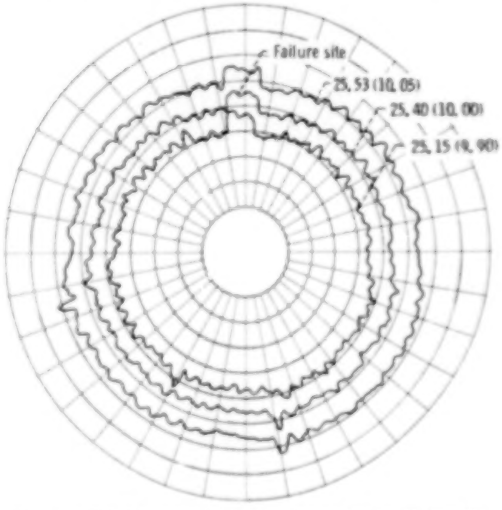

(d) Postfailure data for heat-treated Amzirc thrust chamber 82 after 250 cycles.

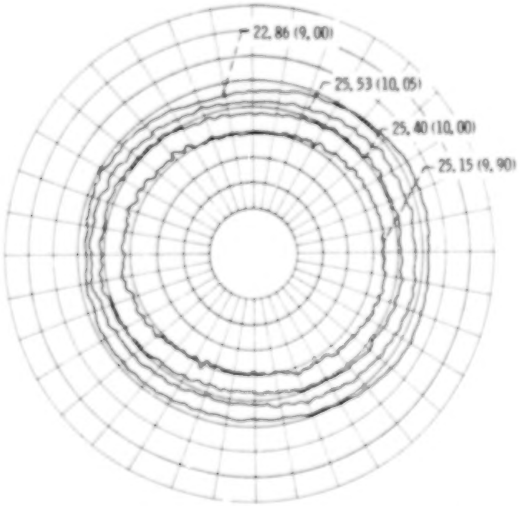

(e) Intermediate-life data for heat-treated Amzirc chamber 82 after 99 cycles.

Figure 8. - Polar plots showing hot-gas-side wall deformation.

nondestructive, it was also employed to obtain deformation data at intermediate-life points. Two variations of the nondestructive method were used. First, the 360° plots previously described could be made at various axial locations, but that required removing the chambers from the thrust stand. Second, it was found that, after the most highly deformed area had been located, data could be taken from plaster casts of the area. Examples of intermediate-life hot-gas-side wall deformation data are shown in figure 8(b) for OFHC copper chamber 74 after 124 cycles and in figure 8(e) for heat-treated Amzirc chamber 82 after 99 cycles. The polar plots were made at various axial stations near the most highly deformed area. The potential failure site can readily be identified for OFHC copper chamber 74 even though the failure did not occur for another 69 cycles. The double-bump characteristic is also evident. As can be seen from table I there was good agreement between deformation data taken with the two methods for OFHC copper chamber 74 at 124 cycles. The 360° plots indicated a deformation of 0.173 millimeter (0.0068 in.) and the plaster cast method indicated a deformation of 0.155 millimeter (0.0061 in.).

A significant observation from the intermediate-life deformation data is that the failure site was identified early in the life of the chamber. For example, with chambers 75 and 82 the potential failure sites were identified before the midlife point. With chamber 74 the failure site was identified just past the midlife point (table I). It is likely that if data had been recorded earlier in the life of these chambers, especially the copper chambers, serial numbers 74 and 75, the failure site could have been identified earlier.

The failure site deformation data for the two OFHC copper chambers (serial numbers 74 and 75) and for the heat-treated Amzirc chamber (serial number 82) are presented in figure 9(a) as functions of accumulated cycles. Where available, data taken with both nondestructive methods, that is, plaster cast segments and full 360° plots, are shown. The closed symbols are the postfailure points and represent an average of the nondestructive and the postfailure photographic data. Even as the deformation becomes large, the failure site bulges out into the chamber in a nearly linear manner as cycles are accumulated. Reference 5 has characterized the failure mechanism as a ratcheting type of process. The slope of the deformation histories presented in figure 9 could be considered a ratcheting rate. The ratcheting rate is nearly three times greater for the OFHC copper than for the heat-treated Amzirc. As noted in the Apparatus section, the structural jackets for the OFHC thrust chambers

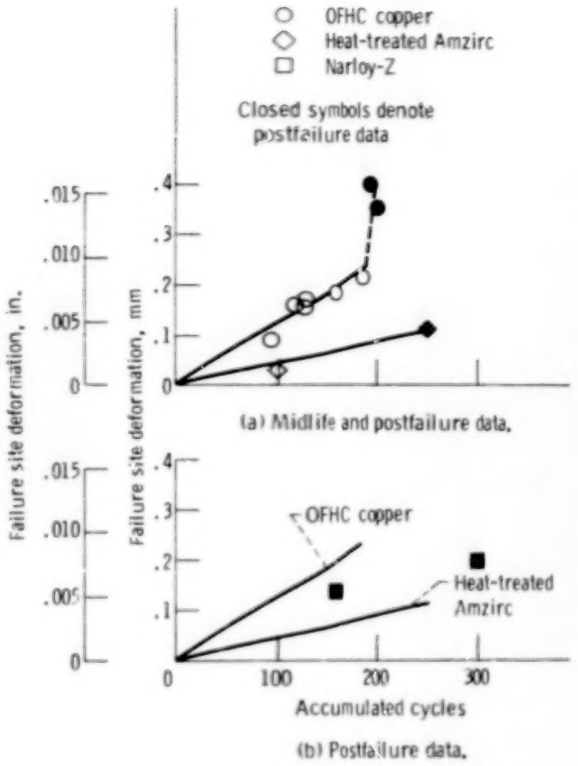

Figure 9. - Failure site deformation as a function of accumulated cycles for three different thrust chamber liner materials.

were not as stiff as the other chamber jackets. It was reported in reference 6 that the low-stiffness structure reduced the strain range approximately 10 percent below that for the thick nickel structure. Consequently, if the OFHC chambers had been fabricated with higher stiffness like the Narloy-Z and Amzirc chambers, the trend would be toward increasing the ratcheting rate for the OFHC copper.

As shown by the dashed line in figure 9(a) there was a rapid increase in the hot-gas-side wall deformation just before failure with the OFHC copper chamber. At the onset of failure the material no longer ratchets linearly but becomes unstable and rapidly deforms (thins) until a tensile stress failure occurs. This was seen visually in the cross-sectional photograph (fig. 7(a)) as local necking of the material adjacent to the crack. The rapid deformation and thinning may have occured in the final cycle or progressively during the last nine cycles.

The ratcheting rate curve is not as well defined for the heat-treated Amzirc as for the OFHC copper. A linear curve was drawn through the origin and the single midlife data point. This curve was extrapolated to 250 cycles. Since the postfailure data are close to this linear ratcheting rate curve, the indication was that the material does not rapidly deform at the onset of failure.

As was stated earlier the cross-sectional photographs of the heat-treated Amzirc and the Narloy-Z failure sites did not indicate local necking of the material adjacent to the crack. The postfailure deformation data for the two Narloy-Z thrust chambers are shown in figure 9(b) along with the deformation histories for the OFHC copper and heat-treated Amzirc chambers presented above. A single deformation rate curve could be used for both Narloy-Z chambers but with failure occurring at different points.

It appears that the ratcheting rate is unique for each material and that the ratcheting rate of the failure site is nearly constant. (The ratcheting rate is of course greater at the failure site than at any other site in the chambers.) For the two Narloy-Z chambers the ratcheting did not proceed for the same number of cycles before a failure occurred. The ratcheting rate data in figure 9 are for a specific set of operating conditions and geometry and therefore do not have universal application. But if early identification of failure sites and ratcheting rate can be applied to a failure mechanism that relates to minimum wall thickness, there is the potential for estimating the remaining cycles to failure.

Correlation of Deformation with Hot-Gas-Side Wall Thinning

The final failure site deformation as a function of the final failure site hot-gas-side wall thickness is shown in figure 10 for three different thrust chamber materials. The data were obtained by measuring cross-sectional photographs. The definition of deformation was the same as that used with the polar plots (fig. 8). The wall thickness was measured as indicated in figure 7. As shown in figure 10 the wall-thickness-versus-deformation data are correlated by a straight line that extrapolates to the original wall thickness of 0.899 millimeter (0.035 in.) for zero deformation. Although this correlation was made from postfailure data, it is assumed that the correlation is also valid at intermediate life. Use of this correlation provides a means for determining wall thickness at intermediate-life points from measurements of hot-gas-side wall deformation.

For example, the use of the correlation between hot-gas-side wall deformation and thinning made it possible to estimate the wall thickness for the OFHC copper at the onset of failure. By extrapolating the OFHC ratcheting rate curve (fig. 9(a)) to 200 cycles it can be seen that at the onset of failure the deformation was approximately 0.25 millimeter (0.010 in.). Figure 10 shows that a 0.25-millimeter (0.010-in.) deformation corresponds to a wall thickness of 0.475 millimeter (0.0187 in.).

Effect of Deformation on Wall Temperature

Any changes in the strain and/or thermal cycles that are caused by the progressive deformation (ratcheting) of the hot-gas-side wall during cyclic testing would be of interest in developing comprehensive models for thrust chamber life prediction. The effect of three types of deformation on the hot-gas-side wall temperature was predicted analytically and compared with experimental data. The types of deformation considered were (1) bulging of the coolant channel wall toward the thrust chamber centerline, (2) thinning of the coolant channel wall, and (3) roughening of the hot-gas-side wall surface. All three types of deformation have been observed experimentally.

The effect of bulging on the hot-gas-side wall temperature was predicted by using an in-house rocket evaluation computer program based on previous rocket experience. This evaluation program has been used extensively to predict hot-gas-side wall temperature, coolant-side wall temperature, coolant pressure drop, etc., for a given thrust chamber geometry. The coolant channel bulge was modeled as being a simple increase in the coolant channel cross section in the plane of the throat. As a reference case the experimentally determined deformation (bulge) for OFHC copper chamber 74 at 184 cycles was used (table I). The deformation was 0.216 millimeter (0.0085 in.). Throat plane dimensions for the baseline and for the bulged configuration are shown

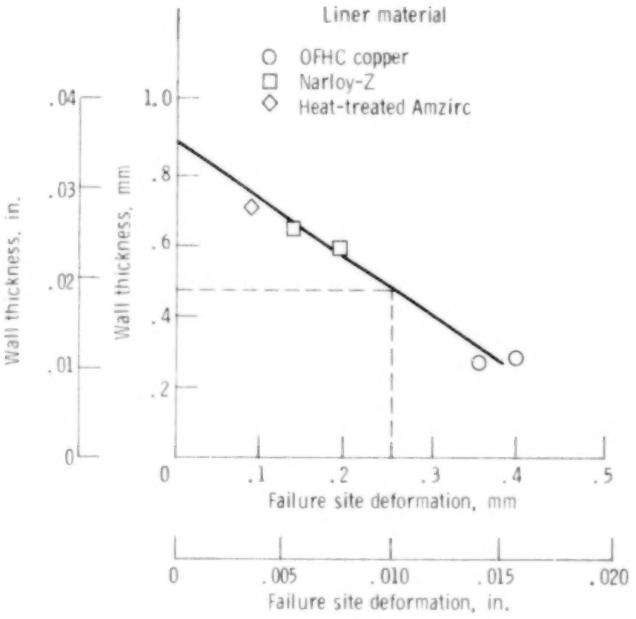

Figure 10. - Failure site deformation as a function of coolant channel wall thickness for three different thrust chamber liner materials.

in table II. The increase in the coolant channel cross-sectional area was computed to be approximately 4 percent for the bulged coolant channel shape. Therefore the model for the bulge was a rectangular cross section of 4 percent larger cross-sectional area and with the channel width and wall thickness equal to those of the baseline configuration. The evaluation computer program predicts that the effect of the bulge would be to increase the hot-gas-side wall temperature 13 K (24 deg R) above the baseline temperature.

The effect of coolant channel wall thinning on the hot-gas-side wall temperature was also predicted by using the rocket evaluation computer program. The wall thickness corresponding to the 0.216-millimeter (0.0085-in.) deformation for OFHC copper chamber 74 was determined to be 0.533 millimeter (0.021 in.) by using the deformation-wall thickness correlation presented in figure 10. As shown in table II the throat plane model for the effect of wall thinning was identical to the baseline case except for the thickness of the hot-gas-side wall. The effect of wall thinning was to decrease the hot-gas-side wall temperature 25 K (45 deg R) below the baseline temperature.

The combination of bulging and thinning of the coolant channel wall as cycles are accumulated has only a small effect on the hot-gas-side wall temperature, even for the large deformation that occurred with the OFHC chambers just before failure. For the OFHC copper chamber 74 the net effect was a predicted decrease in hot-gas-side wall temperature of only 13 K (21 deg R) for a deformation of 0.216 millimeter (0.0085 in.).

The hot-gas-side surface of rocket thrust chambers that have been subjected to cyclic testing has been observed to roughen. This roughness, which is distinctly different from the deformation previously discussed, has been described as having an orange peel appearance. When coolant channel rib temperature and/or coolant temperature data have been available, significant increases in temperature have been reported as cycles were accumulated (ref. 5). If it is assumed from the previous discussion that these increases in temperature were not predominantly the result of bulging, the increases were possibly due to the roughening. Of the five

TABLE II. - THROAT DIMENSIONS

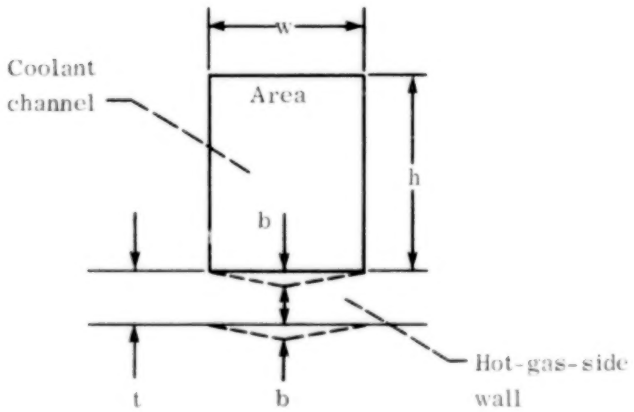

Throat plane configuration	w		h		t		b		Area	
	mm	in.	mm	in.	mm	in.	mm	in.	mm^2	in^2
Baseline	2.24	0.088	2.946	0.1160	0.889	0.035	0	0	6.5990	0.01021
Bulged	↓	↓	2.946	.1160	.889	.035	[a].2159	[a].0085	6.8410	.01203
Bulged model			3.054	.1203	.889	.035	0	0	6.8410	.01203
Thinned model			2.946	.1160	[b].533	[b].021	0	0	6.5990	.01021

[a]Experimental data with OFHC copper chamber 74 at 184 cycles (table I).

[b]Wall thickness obtained from fig. 10 for 0.2159-mm (0.0085 in.) deformation.

thrust chambers reported in the present work the measured rib temperature was observed to increase significantly in only one. The rib temperature measured in the plane of the throat for heat-treated Amzirc chamber 82 increased 77 K (138 deg R) over the life of the chamber. Little or no increase was observed with either the two Narloy-Z or the two OFHC copper chambers.

Previously unpublished data obtained during the life testing with an OFHC copper chamber in reference 5 are presented in figures 11 and 12 to further illustrate the effect of surface roughness on the hot-gas-side wall temperature. Increases in the measured rib temperature (fig. 11), the coolant pressure drop, and the coolant temperature rise (fig. 12) were reported for an OFHC copper chamber with a thick electroformed nickel closeout similar to the Narloy-Z chambers in the present work. The roughening progressed and the temperatures increased as 60 cycles were accumulated. In an attempt to link the surface roughening effect to the increasing temperature effect the hot-gas-side wall was polished with a fine-grit emery paper by rubbing only in the axial direction. The effect of this

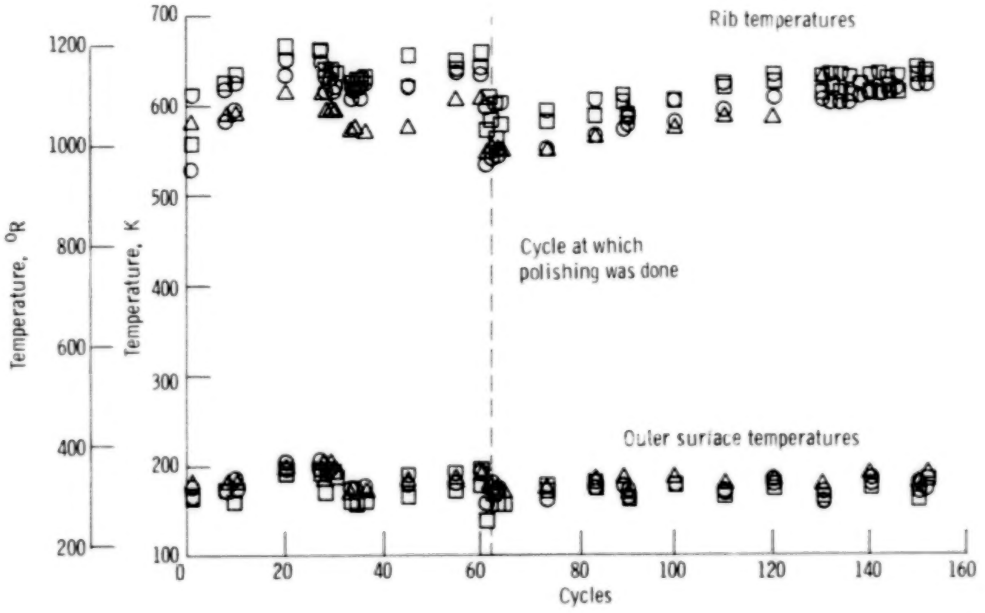

Figure 11. - Effect of polishing hot-gas-side wall surface on wall temperatures - OFHC thrust chamber 70.

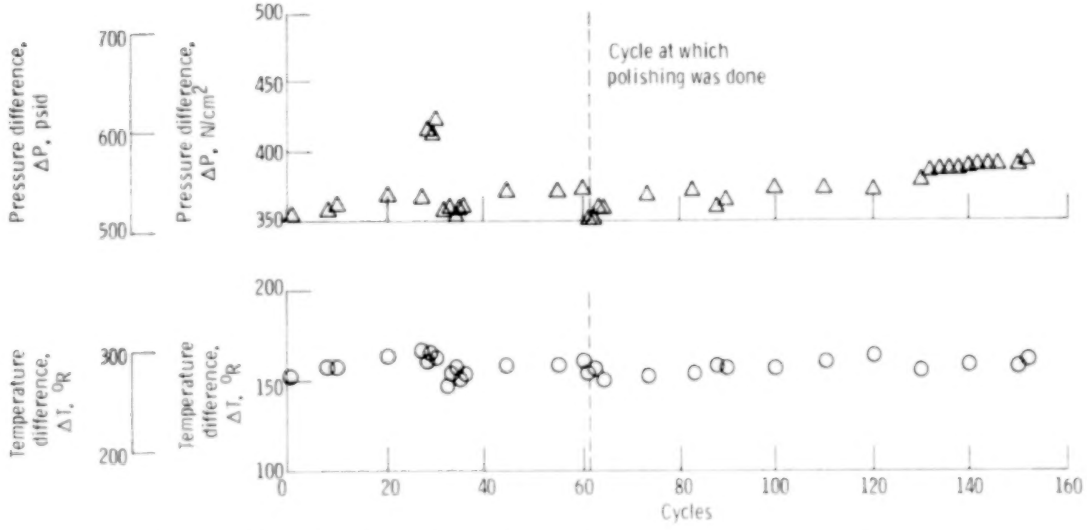

Figure 12. - Effect of polishing hot-gas-side wall surface on coolant temperature and pressure differences - OFHC thrust chamber 70.

polishing can also be seen in figures 11 and 12. The average rib temperature for the sixty-first cycle was approximately 83 K (150 deg R) less than that for the sixtieth cycle. Similar changes can be seen in other parameters. The polishing did not remove the deformation (bulging of the coolant channel) but instead restored the surface finish to approximately the original condition. The resumption of cyclic testing again caused the temperatures to steadily increase. After the chamber had been tested for a total of 153 cycles the hot-gas-side surface roughness (in the axial direction) was measured. The roughness was 230×10^{-6} to 760×10^{-6} centimeter rms (90×10^{-6} to 300×10^{-6} in. rms).

Surface roughness has been shown to affect the hot-gas-side heat transfer coefficient h_g. Reference 12 shows that the heat transfer coefficient for a rough surface, 826×10^{-6} centimeter rms (325×10^{-6} in. rms), is 25 percent greater than that for a smooth surface. Local surface roughness was measured in the throat plane of OFHC copper chamber 70 after 153 cycles and found to be nearly as high as the surface roughness reported in reference 12. By using a thermal analysis computer program, SINDA, the h_g's corresponding to both smooth- and rough-wall rib temperature data were determined. (For a more complete description of SINDA and the specific use in the present work, see the appendix.) The h_g corresponding to the rough wall was 24 percent greater than that for the smooth wall. The rough wall produces a rib temperature (and also a hot-gas-side wall temperature 84 K (151 deg R) higher than does either the original or the polished wall. These results are consistent with the reference 12 results for the effect of surface roughness on the hot-gas-side heat transfer coefficient.

If hot-gas-side surface roughening does occur, the deformation rate may tend to increase because of the increasing temperature. Also, if the hot-gas-side roughening occurs, polishing would seem to lengthen the life; but this was not demonstrated with chamber 70. Chamber 70 was one of four identical chambers that were cycled to failure in reference 5. The polished chamber failed after 152 cycles. The other three chambers failed at 165, 130, and 151 cycles.

The effects of roughening on wall temperature have been presented here, but the circumstances that cause roughening were not studied. In general, the roughening occurs in the hottest and/or the highest strain locations. Roughening has been observed in all the high-conductivity copper and copper-based alloy materials tested in thrust chambers and has also been observed in hourglass test specimens used in materials testing. The cause of this roughening is not understood, but it is hypothesized that it contributes to the ratcheting process described earlier by increasing the hot-gas-side heat transfer coefficient and in turn the wall temperature.

Discussion of Failure Mechanism

As noted in reference 4 and as can be seen in figure 8(a) of the present work the visual evidence supports the contention of tensile stress failure with OFHC copper. For a tensile stress failure to occur the ultimate stress for the material must be exceeded at some point in the cycle. The exact point in the cycle when failure occurred is not known since both the stress in the wall and the ultimate stress of the material are changing with time. The stress is nominally the same for all three materials for the same wall thickness and would increase as the wall thickness decreases. Therefore it is assumed that a wall thickness of approximately 0.475 millimeter (0.0187 in.) corresponds to a stress in the wall equal to the ultimate stress value of OFHC copper. The result is a tensile stress failure. However, since the published data for heat-treated Amzirc and Narloy-Z indicate that the ultimate stress is greater than that for OFHC copper at similar temperature conditions, the level of stress in a wall 0.475 millimeter (0.0187 in.) thick would not produce a tensile stress failure in these stronger materials. Figure 10 shows that these stronger materials possibly failed at even lower stress levels than did the OFHC copper since the final wall thickness was greater than with OFHC copper. The implication is that the failure mechanism for the heat-treated Amzirc and Narloy-Z thrust chambers in the present work is more complicated than simple tensile stress failure and probably includes a crack-producing mechanism such as fatigue.

Summary of Results

A test program was conducted to investigate the deformation and surface roughening of five rocket thrust chambers subjected to cyclic testing. Two of the thrust chambers were fabricated from oxygen-free, high-conductivity (OFHC) copper, two were fabricated from Narloy-Z, and one was fabricated from heat-treated Amzirc. The propellants used were gaseous hydrogen and liquid oxygen. A separate flow of liquid hydrogen was used as the thrust chamber coolant. The combustion chamber pressure was 4.14 MN/m^2 (600 psia). The throat diameter was 6.60 centimeters (2.60 in.). The following results were obtained:

1. A cyclic-induced deformation, ratcheting, was present in thrust chambers fabricated from OFHC copper, Narloy-Z, and heat-treated Amzirc. The ratcheting continued until a crack was produced in

the hot-gas-side wall.

2. Ratcheting rates were determined experimentally, and OFHC copper was found to have a higher rate than heat-treated Amzirc.

3. Ratcheting rate was found to be nearly linear throughout the life of both OFHC and heat-treated Amzirc chambers.

4. Hot-gas-side wall deformation was correlated with hot-gas-side wall thinning by a single straight line.

5. The potential failure site could be identified near midlife by using nondestructive methods to monitor deformation of the hot-gas-side surface.

6. The failure mechanism observed with OFHC copper thrust chambers was consistent with the stress rupture type of mechanism described by Quentmeyer (AIAA paper 77-843). But, the failure mechanism with the heat-treated Amzirc and Narloy-Z thrust chambers appeared to be more complicated than simple tensile stress failure.

7. OFHC copper strain softened and Narloy-Z and heat-treated Amzirc strain hardened as cycles were accumuated.

8. The combination of bulging and thinning of the coolant channel wall has only a small effect on the hot-gas-side wall temperature.

9. Roughening of the hot-gas-side surface as a result of cyclic testing increased the hot-gas-side heat transfer coefficient by 24 percent. The effect of roughening was reversed by polishing the thrust chamber wall.

Lewis Research Center
National Aeronautics and Space Administration
Cleveland, Ohio, October 8, 1980

Appendix—Description of Thermal Analysis Computer Programs

Two thermal computer programs were used to study the effects of deformation and surface roughening on the temperature of the rocket thrust chamber wall. These programs, a finite difference computer program called SINDA and a rocket evaluation computer program, have been used extensively in a variety of research programs. SINDA (ref. 13) was used to calculate transient, two-dimensional heat transfer in this study. This program requires the establishment of a nodal system to describe the geometry of a cross section.

Inputs required for the program include the coolant-side heat transfer coefficient h_c, the adiabatic wall temperature T_{aw}, the coolant temperature T_c, and the hot-gas-side heat transfer coefficient h_g. The coolant-side heat transfer coefficient can be varied around the coolant channel. All the inputs can be functions of time to simulate the thermal transients. The analytical model for the throat plane cross section is shown in figure 13. Shown is a radial cross section of 3° arc. The section includes the hot-gas-side wall, the coolant passage, and the remaining closeout structure. Because of symmetry this section is sufficient to model the entire cross section of the thrust chamber in the plane of the throat. Also shown in the figure is the nominal location of one of 16 rib temperature instrumentation stations (four axial stations each at four equally spaced circumferential locations). An outer wall thermocouple was located near each rib temperature thermocouple, as shown in figure 13.

The rocket evaluation computer program was used in the study to determine the steady-state values of T_{aw}, T_c, h_g, and h_c for inclusion in the SINDA program. This steady-state program is an in-house rocket evaluation computer program that has been used extensively and is based on previous rocket experience. This program will predict the hot-gas-side wall temperature, the coolant-side wall temperature, the coolant pressure drop, h_c, h_g, etc., for a given thrust chamber geometry.

Experimental values of rib temperature (measured 1.27 mm (0.050 in.) from the hot-gas-side wall) and outer wall temperatures are shown in figure 14 as functions of time. It can be seen that the rib temperature reached a steady-state value. Of more interest, however, was to obtain a plot of the hot-gas-side wall temperature T_{gw} as a function of time. SINDA was used to predict T_{gw}, but it was necessary to describe T_{aw}, h_g, and h_c as functions of time. The final steady-state values were predicted by the in-house rocket evaluation program, but proper values during the transient were found by trial-and-error comparisons of the measured rib temperature and the predicted temperature at the nominal location of the thermocouple. Also shown in figure 14 are the predicted curves for the hot-gas-side wall temperature, the rib temperature, and the outer wall temperature.

The values of h_g and h_c that were used to predict the smooth-wall cases in the study are shown in figure 15. The adiabatic wall temperature was assumed to be the steady-state value at time zero. Because of the change in temperature of the hydrogen coolant as a test progressed, the h_c changed in value from the start of a cycle to the steady-state running condition. This change was due to the variation of transport properties with

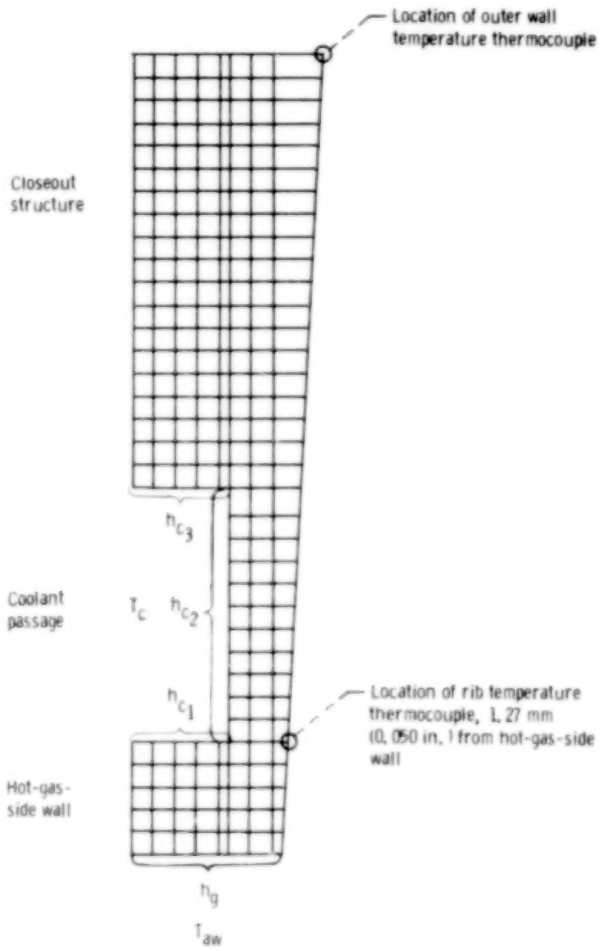

Figure 13. - Analytical cross-sectional thermal model of rocket combustor at instrumented location.

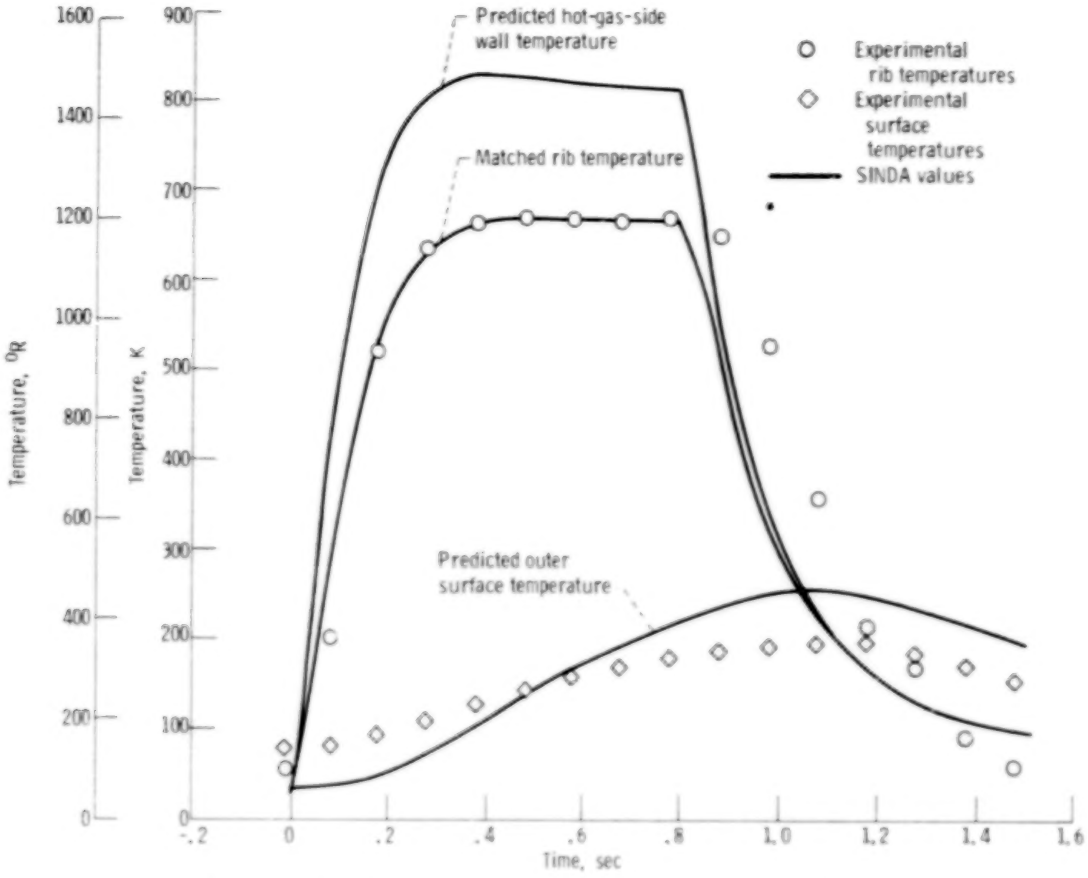

Figure 14. - Predicting hot-gas-side wall temperatures from measured temperatures.

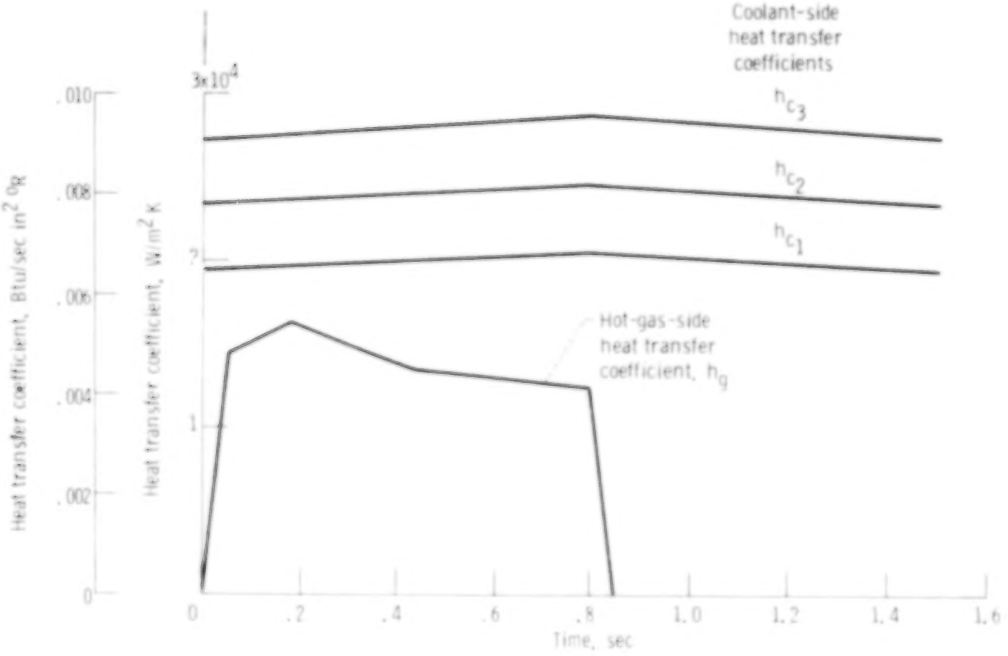

Figure 15. - Heat transfer coefficient as a function of time.

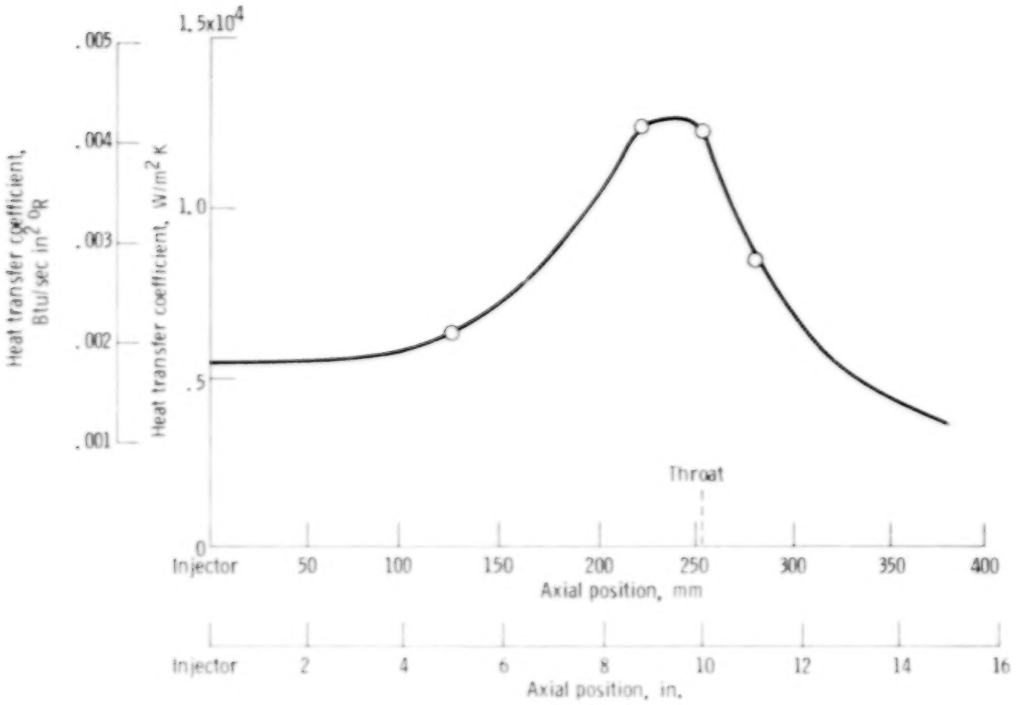

Figure 16. - Heat transfer coefficients as a function of axial position.

temperature. A 5 percent decrease in h_c was used at the start of the cycle and then again at the end of the cycle with a linear distribution between, as shown in figure 15.

The relationship between the h_c's used in the analysis was as follows:

$$h_{c2} = 1.2\ h_{c1}$$

$$h_{c3} = 1.4\ h_{c1}$$

These differences were also due to the difference in transport properties as a function of temperature. Figure 16 shows the axial distribution at steady-state conditions of h_g for the thrust chamber at the four instrumented stations.

References

1. Fulton, D.: Investigation of Thermal Fatigue in Non-Tubular Regeneratively Cooled Thrust Chambers, Vol. 1. R-9093-Vol. 1, Rockwell International Corp., 1973. (AD-760582; AFRPL-TR-73-10-Vol. 1.)
2. Fulton, D.: Investigation of Thermal Fatigue in Non-Tubular Regeneratively Cooled Thrust Chambers, Vol. 2. R-9093-Vol. 2, Rockwell International Corp., 1973. (AD-760583; AFRPL-TR-73-10-Vol. 2.)
3. Armstrong, W. H.: The 3.3 K Thrust Chamber Life Prediction. (D180-18170-1, Boeing Aerospace Co.; NASA Contract NAS8-30615.) NASA CR-144048, 1974.
4. Quentmeyer, R. J.: Experimental Fatigue Life Investigation of Cylindrical Thrust Chambers. AIAA Paper 77-893, July 1977. (Also NASA TM X-73665, 1977.)
5. Hannum, N. P.; Kasper, H. J.; and Pavli, A. J.: Experimental and Theoretical Investigation of Fatigue Life in Reusable Rocket Thrust Chambers. AIAA Paper 76-685, July 1976. (Also NASA TM X-73413, 1976.)
6. Kasper, H. J.; and Notardonato, J. J.: Effect of Low Stiffness Closeout Overwrap on Rocket Thrust-Chamber Life. NASA TP-1456, 1979.
7. Quentmeyer, R. J.; Kasper, H. J.; and Kazaroff, J. M.: Investigation of the Effect of Ceramic Coatings on Rocket Thrust Chamber Life. AIAA Paper 78-1034, July 1978. (Also NASA TM-78892, 1978.)
8. The JANNAF Rocket Engine Performance Prediction and Evaluation Manual. CPIA-PUBL-246, Chemical Propulsion Information Agency, Johns Hopkins U., 1975.
9. Conway, J. B.; Stentz, R. H.; and Berling, J. T.: High Temperature, Low-Cycle Fatigue of Copper-Base Alloys in Argon. Part I: Preliminary Results for 12 Alloys at 1000° F (538° C). (Mar-Test, Inc.; NASA Contract NAS3-16753.) NASA CR-121259, 1973.
10. Conway, J. B.; Stentz, R. H.; and Berling, J. T.: High Temperature, Low-Cycle Fatigue of Advanced Copper-Base Alloys for Rocket Nozzles; Part I—Narloy-Z. (MTI-R003-3-1, Mar-Test, Inc.; NASA Contract NAS3-17777.) NASA CR-134627, 1974.
11. Armstrong, W. H.: Structural Analysis of Cylindrical Thrust Chambers (LMSC-HREC-TR-D568827-VOL-1, Lockheed Missiles and Space Co.; NASA Contract NAS3-21361.) NASA CR-159522, 1979.
12. Boldman, D. R.; and Graham, R. W.: Heat Transfer and Boundary Layer in Conical Nozzles. NASA TN D-6594, 1972, p. 30.
13. Smith, J. P.: Systems Improved Numerical Differencing Analyzer (SINDA): User's Manual. (TRW-14690-H001-R0-00, TRW Systems Group; NASA Contract NAS9-10435.) NASA CR-134271, 1971.

1. Report No. NASA TP-1834	2. Government Accession No.	3. Recipient's Catalog No.
4. Title and Subtitle SOME EFFECTS OF THERMAL-CYCLE-INDUCED DEFORMATION IN ROCKET THRUST CHAMBERS		5. Report Date April 1981 6. Performing Organization Code 506-52-12
7. Author(s) Ned P. Hannum and Harold G. Price, Jr.		8. Performing Organization Report No. E-553
9. Performing Organization Name and Address National Aeronautics and Space Administration Lewis Research Center Cleveland, Ohio 44135		10. Work Unit No. 11. Contract or Grant No.
12. Sponsoring Agency Name and Address National Aeronautics and Space Administration Washington, D.C. 20546		13. Type of Report and Period Covered Technical Paper 14. Sponsoring Agency Code
15. Supplementary Notes		

16. Abstract

A test program to investigate the deformation process observed in the hot-gas-side wall of rocket combustion chambers was conducted for three different liner materials. Five thrust chambers were cycled to failure by using hydrogen and oxygen as propellants at a chamber pressure of 4.14 MN/m^2 (600 psia). The deformation was observed nondestructively at midlife points and destructively after failure occurred. The cyclic life results are presented with an accompanying discussion about the problems of life prediction associated with the types of failures encountered in the present work. Data indicating the deformation of the thrust chamber liner as cycles are accumulated are presented for each of the test thrust chambers. From these deformation data and observation of the failure sites it is evident that modeling the failure process as classic low-cycle thermal fatigue is inadequate as a life prediction method. The stress rupture model that has been proposed may apply to oxygen-free, high-conductivity (OFHC) copper but not to the other materials that were tested. Also, the effects of deformation and surface roughening on rocket thrust chamber wall temperatures were studied by using a thermal analysis computer program.

17. Key Words (Suggested by Author(s))	18. Distribution Statement
Thrust chambers Cyclic induced deformation Wall roughness Reusability	Unclassified - unlimited STAR Category 20

19. Security Classif. (of this report)	20. Security Classif. (of this page)	21. No. of Pages	22. Price*
Unclassified	Unclassified	23	A02

* For sale by the National Technical Information Service, Springfield, Virginia 22161

NASA-Langley, 1981

90 %

50 %

END

6-11-81